Unlocking sustainable cooling: a numerical analysis of ice slurry flow in 180° U-bends-impacts of bend radius/pipe radius ratios and pressure drops on system performance

Q2 Q3 Q4 Q5

The corrections made in this section will be reviewed by journal production editor.

Kamal Singh Rawat, Prabhakar Bhandari, prabhakar.bhandari40@gmail.com, Vijay Singh Bisht, ~~N.~~ BeemkumarNagappan~~, n.beemkumar@jainuniversity.ac.in~~, Lalit Ranakoti, Karthikeyan ~~A.~~Alagu~~, akarthikeyan.auto@sathyabama.ac.in~~, Dhirendra Nath Thatoi~~, dhirendrathatoi@soa.ac.in~~, Shubham Sharma, shubham543sharma@gmail.com, V. Nagabhushana Rao~~, nagabhushanarao.v@raghuenggcollege.in~~ and Ehab El Sayed Massoud~~, ehabheca@gmail.com~~

Department of Mechanical Engineering, MIET, Meerut, Uttar Pradesh, India

Department of Mechanical Engineering, School of Engineering and Technology, K. R. Mangalam University, Gurgaon, Haryana, India

Faculty of Technology, Department of Thermal Engineering, Veer Madho Singh Bhandari Uttarakhand Technical University, Dehradun, Uttarakhand, India

Department of Mechanical Engineering, School of Engineering and Technology, JAIN (Deemed to be University), Bangalore, Karnataka, India

Department of Mechanical Engineering, Graphic Era to be Deemed, Dehradun, 248002, India

Department of Mechanical Engineering, Sathyabama Institute of Science and Technology, Chennai, Tamil Nadu, India

Department of Mechanical Engineering, Siksha 'O' Anusandhan (Deemed to be University), Bhubaneswar, Odisha-751030, India

Department of Technical Sciences, Western Caspian University, Baku, Azerbaijan

Centre for Research Impact and Outcome, Chitkara University Institute of Engineering and Technology, Chitkara University, Rajpura-140401, Punjab, India

Jadara University Research Center, Jadara University, Jordan

Department of Mechanical Engineering, Raghu Engineering College, Vishakhapatnam-531162, Andhra Pradesh, India

College of Applied Sciences, King Khalid University, Dhahran Al-Janoub, Abha, Kingdom of Saudi Arabia

Corresponding authors: Prabhakar Bhandari, Department of Mechanical Engineering, School of Engineering and Technology, K. R. Mangalam University, Gurgaon, Haryana, India, E-mail: prabhakar.bhandari40@gmail.com; and **Shubham Sharma**, Department of Technical Sciences, Western Caspian University, Baku, Azerbaijan; Centre for Research Impact and Outcome, Chitkara University Institute of Engineering and Technology, Chitkara University, Rajpura-140401, Punjab, India; and Jadara University Research Center, Jadara University, Jordan, E-mail: shubham543sharma@gmail.com, shubhamsharmacsirclri@gmail.com

Department of Mecha.nical Engineering, Graphic Era to be Deemed, Dehradun, 248002, India

Abstract

Ice slurry serves as an effective secondary-loop refrigerant, boosting system performance while simultaneously minimizing refrigerant charge and leakage. This not only enhances energy efficiency but also addresses environmental safety concerns. Unlike single-phase flow, ice slurry exhibits complex multi-phase dynamics, making its behavior in pipelines distinctly different. Since bend sections are essential for flexible routing in pipeline transportation, they also significantly influence the flow characteristics. In this study, the flow behavior of ice slurry within bend sections has been thoroughly examined. The investigation has been performed in 23 mm diameter pipe with 180° bend section with 2 different (Bend radius/Pipe radius) ratios of 2.98 & 5.6. The Eulerian multi-phase based CFD model is developed for the investigation which is first validated with literature. Investigation has been done for ice concentrations of 10, 20 and 30 % by volume at 1 m/s to 3 m/s velocities, and particles diameters of 0.25 mm and 0.40 mm. From the investigation, it has been observed that, concentration and velocity distributions are affected in bend section. The concentration exhibits a rising trend from the inner section toward the outer section of the bend, as well as along the upper region of the pipe. Additionally, an increase in the *R*/*r* ratio from 2.98 to 5.60 leads to a reduction in pressure drop by up to 9 %. This indicates that as the relative size changes, there is a noticeable decrease in pressure drop, suggesting a potential correlation between the radius ratio and fluid resistance or flow characteristics.

Keywords Eulerian; bend pipe; ice slurry; CFD; bend ratios; pressure drop

Nomenclature

$\vec{g}$ Gravitational acceleration

$\overline{\overline{I}}$ Unit tensor

$\vec{R}$ Interfacial forces

K Liquid Solid exchange coefficient

$\vec{F}_D$ Drag Force

$\vec{F}_{\text{lift}}$ Lift force

C_L Lift force coefficients

C_D Drag force coefficients

C_{TD} Turbulent dispersion force coefficients

C Ice concentration

d_s Solid particle diameter

D Pipe diameter

e_{ss} Particle-particle coefficient of restitution

e_{sw} Particle-wall coefficient of restitution

$\vec{v}$ Velocity

P Pressure

Re Reynold Number

K_{θ_s} Coefficient of diffusion

V Flow velocity

Abbreviations

SLR Secondary Loop Refrigeration

FPD freezing point depressant

SIMPLE Semi-Implicit Method for Pressure Linked Equations

QUICK Quadratic Upstream Interpolation for Convective Kinematics

KTGF Kinetic Theory of Granular Flow

Y Y axis variation along

v_s' Particle fluctuating velocity

Greek Symbol

α Volume fraction

ρ Density

μ Viscosity

μ_t Turbulence viscosity

γ_{θ_s} Collisional dissipation of energy

λ Bulk viscosity

τ Shear stress

σ_{sl} Dispersion Prandtl number

θ_s Granular temperature

ϕ_{ls} Energy exchange between S-L phase

ψ Specularity coefficient

Subscript

S Solid

L Liquid

col Collision

kin Kinetic

CFD Computational Fluid Dynamics

VOF Volume of Fluid

1 Introduction

In the wake of alarming depletion of conventional resources, the world's focus has been directed towards improving the efficiency of day-to-day appliances or switching to unconventional resources. In particular, during summer months, most of the energy consumption is linked to refrigeration and air-conditioning systems, which are also environmentally problematic. To combat these problems, the use of secondary loop refrigeration (SLR) in combination with cold storing systems proves to be a beneficial option [1], [2]. The SLR systems utilize either a one-phase or a two-phase work fluid as the refrigerant. The use of a two-phase fluid flow presents advantages of larger heat transfer, along with uniformity in the temperature, exploiting the latent heat in the course of the process of phase transformation.

The application of an ice slurry system is a novel and effective method in many industries, demonstrating its flexibility and applicability. This advanced technology is the process of developing a slushy mixture of ice crystals and a freezing substance, usually water or brine. The system is commonly applied in various fields including food preservation, medical uses, and industrial processes. In the food sector, ice slurry is used for quick freezing and cooling to maintain the quality and safety of perishable foods. In the medical field, it is used for therapeutic cooling in hyperthermia or in some medical procedures. The industrial sector also gains from ice slurry systems by improving energy efficiency in refrigeration and air conditioning systems, resulting in lower energy consumption and environmental footprint. The flexibility of the ice slurry system highlights its relevance in solving various problems in various fields, rendering it a desirable and sustainable technology solution. For SLR cold storage systems that employ ice, employing a slurry of fine ice particles (commonly with an average particle diameter of 0.10 mm or more) and an aqueous solution is beneficial. This slurry is utilized in two capacities as a thermal energy storage medium and secondary refrigerant. The water-based solution is made by mixing water with a freezing point depressant (FPD) to reduce the freezing point of the ice slurry. The FPD also helps to enhance the transport ability of the ice slurry by reducing the roughness of the ice particle surface [3], [4]. Different aqueous solutions, such as NaCl-water, ethanol-water, and ethylene glycol-water solutions, are utilized for this intention [5], [6].

The passage explains how the flow of ice slurry in pipes is a complex process involving two different phases – liquid and solid. Because of lower density, the ice particles will tend to get deposited on the top surface of the pipe in the case of slurry flow, leading to non-uniform ice concentration along the radial direction [7]. The flow behavior of ice slurry is affected by both geometric factors, such as pipe diameter, length, roughness, bends, and operating factors like inlet velocity, particle concentration, particle size, and freezing point depressant (FPD) concentration. Predicting pressure drop, velocity, and particle distribution in ice slurry flow becomes a challenging task due to its dependence on various factors, and these parameters are crucial for evaluating the pumping power required for slurry flow [8].

Recent numerical studies by Cai et al. [9] investigated the impact of different pulsating ice slurry flow (varying amplitude and frequency) in a horizontal pipe. The conclusion drawn was that the use of flow pulsation significantly enhances thermal performance. Several studies have explored different aspects of ice slurry flows, including the determination of pressure drop and rheological characteristics. According to Grozdek et al. [10], ice slurry with an initial ice concentration below 10% can be treated as a Newtonian fluid, while at higher ice concentrations, it must be considered a non-Newtonian fluid. Various rheological models such as Bingham, power law, Cassion, etc., have been employed for ice slurry. Yet, due to the complications of measuring concentration, temperature, and velocity distributions, experimental effort in this domain is limited.

To solve such problems, computational fluid dynamics (CFD) is a potential technique for understanding the physics of fluid flow. CFD is a potent and revolutionary technique in the field of physics and engineering, allowing fluid flow phenomena to be simulated and analyzed. This computer program has transformed the way engineers and researchers investigate the behavior of fluids, including gases and liquids, in different applications. Using numerical algorithms and methods, CFD enables precise prediction and visualization of fluid dynamics, helping to design and optimize complicated systems. In research and development, it is now an indispensable tool that provides economical and efficient ways of solving problems involving fluid flow, heat transfer, and related phenomena. The ongoing progress in computing capability and modeling methods continuously improves the strengths of CFD, making it a must-have for scientists and engineers in solving fluid dynamics problems in diverse fields. The CFD methodology has been widely utilized to simulate flow of slurries of different materials [11]–[14]. While simulating various slurry flows, some of the flow field components require attention, including particle-particle impacts and particle-wall interaction. Two widely employed methods to investigate solid-liquid flows in slurries are the Euler–Lagrange (E-L) and Euler–Euler (E-E) approaches.

In the Euler–Lagrange method, there are numerous solid particles followed in the flow field by considering the liquid phase as a continuum. This method does not consider interaction between solid particles and is therefore more straightforward but inappropriate for ice slurry flow [15], [16]. In contrast, the E-E method considers both the solid and liquid phases as interpenetrating continua. This method has been used before in other flow problems, e.g., sand-water and glass-water interaction [17]. Niezgoda-Zelasko and Zalewski [18] initially applied the E-E method to ice slurry flow in an adiabatic horizontal pipe and obtained good correlation with experimental data, though no calculation on solid fraction distribution was conducted. Wang et al. [19] also carried out a similar study with the Euler–Euler method for isothermal flow of ice slurry through varied pipe configuration. In the E-E method, three model exits are presented:

volume of fluid (VOF), mixture, and Eulerian. Researchers have preferred the use of the mixture model to simulate ice slurry flow, whereas some others have used the Eulerian model [20], [21].

In any branched pipe fluid flow system, bifurcation of flow is a key feature as it helps establish whether or not the flow is evenly or unevenly distributed within a branched pipe. As ice slurry passes through a T-section, it represents a situation similar to that encountered within pipe bends. In a T-section, though, flow is split between two branched pipes. Similar to the flow of a single-phase fluid, there is a pressure drop as the slurry passes through the bent pipe, accompanied by the generation of secondary flow due to centrifugal forces [22]. This secondary flow, in turn, impacts the distribution of ice particles and velocity.

While the majority of research on ice slurry flow has focused on horizontal pipes, only a few researchers have delved into the dynamics of ice slurry flow through pipe bends [23]–[26]. Employing the Population Balance Model (PBM), Cai et al. [27] conducted a numerical investigation of ice slurry flow in a horizontal 90° elbow pipe, revealing that boundary layer separation occurs at a bend angle of 45°. Expanding on this, Ma et al. [28] explored flow behavior for various elbow angles, suggesting that ice slurry transportation systems with elbow angles less than 90° exhibit superior performance. Another study by Cai et al. [29] explored ice slurry flow through helically coiled tubes, observing that an increase in coil radius leads to higher pressure drop, while coil pitch has a minimal influence on pressure drop. Parkash and his group [30]–[33] have performed parametric numerical study for slurry flow (glass beads-water) on horizontal pipe. They studied Prandtl number, solid concentration, flow velocity, wall roughness to optimize the performance. Further, they studied configuration like vertical pipe, horizontal pipe bend [34], [35]. Joshi et al. [36] investigates the flow characteristics of a bi-model slurry system with Silica Sand (SS) and Fly Ash (FA) through a 90° horizontal pipe bend using a computational Eulerian multiphase model. Results show that increasing FA reduces pressure drop, with the 65:35 SS:FA ratio being the most energy-efficient for long-distance slurry transportation. Further, Rezaei and Pakravan [37] investigates the thermo-hydraulic behavior of ice slurry in U-bend pipes using numerical simulations with a multiphase two-fluid model. Results show that heat transfer and pressure drop increase with Reynolds number, ice volume fraction, and particle diameter, with a 76% rise in the Nusselt number when particle diameter triples. Joshi et al. [38] develops a 3D computational model to analyze the transport and thermal behavior of a bi-modal slurry in a 90° pipe bend using an Eulerian-Eulerian approach. There findings indicate that the 65:35 slurry composition minimizes pressure drop, while the 100:0 composition maximizes heat transfer, influenced by fluid viscosity and particle concentration.

Notably, there is a lack of reported research on ice slurry flow through U-shaped pipes to the best of the author's knowledge. Therefore, the primary objective of the proposed work is to gain insights into the fluid flow dynamics through U-shaped sections. Additionally, a comprehensive comparative analysis has been presented and discussed, considering various operating conditions such as flow velocity, ice concentration, and ice particle diameter.

The present research has practical implications in the field of Food and Beverage Industry, Pharmaceutical Industry, Chemical Processing industry, etc. The findings can drive further research into developing new cooling technologies using ice slurry, potentially leading to breakthroughs in refrigeration and cooling systems. The energy efficiency of ice slurry systems makes them suitable for integration with renewable energy sources, contributing to the development of sustainable industrial processes. By optimizing system design and operation based on these findings, manufacturers can achieve significant energy savings, cost reductions, and environmental benefits.

This study introduces several innovative elements, particularly its emphasis on bend sections and the effects of varying R/r ratios, offering practical insights that can enhance the efficiency and performance of refrigeration and cooling systems in real-world applications. While earlier research often concentrated on straight pipeline segments or simpler flow dynamics, this work delves into the complexities associated with a 180° bend, a frequent feature in actual piping systems. By analyzing the influence of different R/r ratios (2.98 and 5.6) on pressure drop, the research presents new findings that can guide the optimization of pipe design to reduce energy losses. This represents a meaningful advancement in the field.

2 Problem description

This study focuses on the flow within a bend pipe, as illustrated in Figure 1, with a diameter of 23 mm and varying R/r (Bend radius/Pipe radius), The pipe features a 180° bend section along with upstream and downstream pipes.

Additional geometric details are provided in Table 1. The examinations specifically concentrate on the behavior within the bend section.

Figure alignment: The figure layout displayed in this section is not how it will appear in the final version. As per journal style, figures will only be left aligned. The presentation below is for the sole purpose of providing corrections to the figures. To view the actual presentation of the figures, please click on the PDF located at the top of the page.

Figure 1:

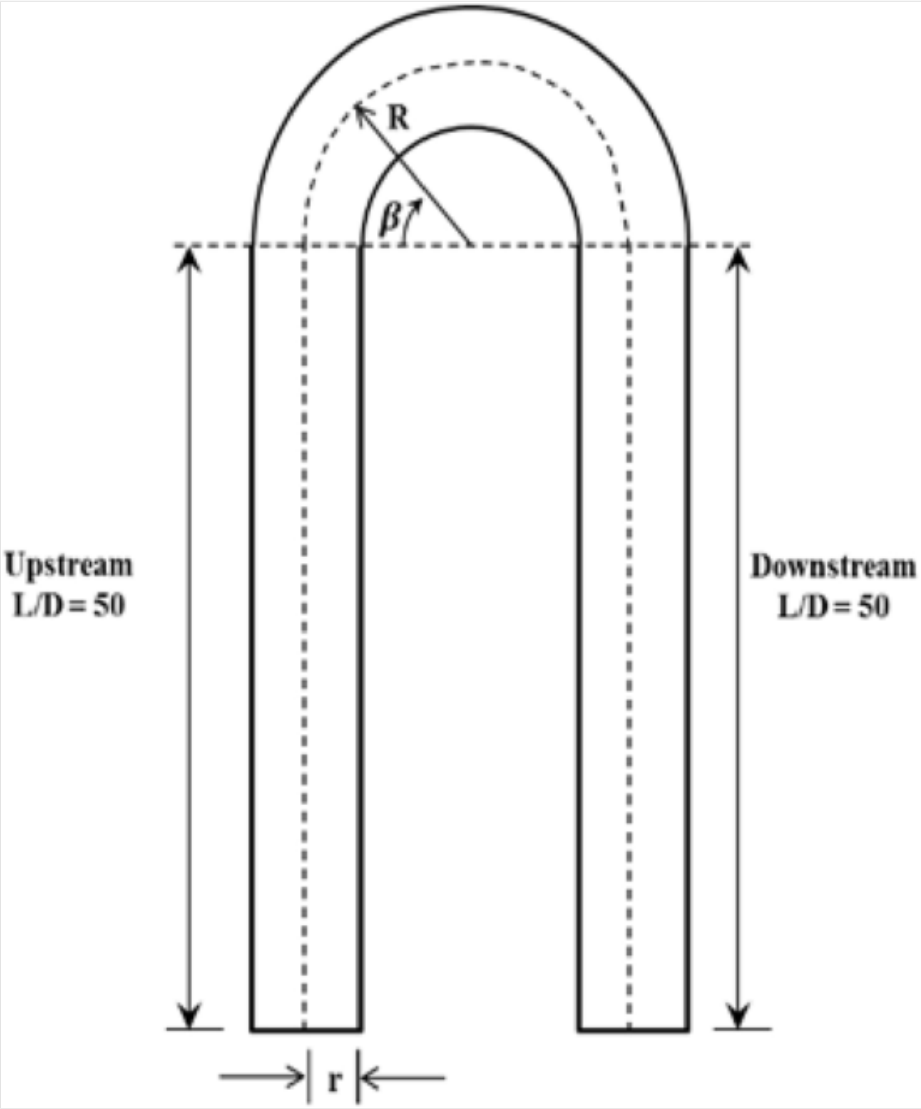

Schematic diagram of 180° U-bend pipe.

Table 1:

The table layout displayed in this section is not how it will appear in the final version. The representation below is solely purposed for providing corrections to the table. To view the actual presentation of the table, please click on the PDF located at the top of the page.

Details of bend pipe geometries.

Pipe geometry	*R*/*r*	*R* (mm)	[a]Bend length (mm)	[a]Total pipe length (m)
180° U-bend pipe	2.98	34.27	107.61	2.40
	5.60	64.40	202.22	2.50

[a]The value is rounded-off after two digits of decimals.

3 Numerical modeling

The modeling of ice slurry flow has been conducted using the Eulerian granular multi-phase approach combined with the per-phase $k-\varepsilon$ turbulence model. The Eulerian approach, while widely used for modeling multiphase flows, has several inherent limitations. The Eulerian approach, which treats different phases as interpenetrating continua, faces difficulties in accurately capturing complex interface dynamics, phase interactions, and large-scale deformations. One of its main disadvantages is the use of averaged equations, which can cause loss of specific information on single particle paths and interface movement. The method also needs strong closure models to consider interphase forces, which introduce uncertainties and numerical complexity. All these renders it less ideal in situations with very dispersed or separated phases such as bubbly or stratified flows. Nevertheless, for current work, it is the most appropriate model. The whole computational domain has been discretized into relatively small volumes, such that every computational elemental volume is greater than the individual particle diameter. The equation of motion has been solved for every phase and averaged across these volumes. In this model, the ice particles are taken to be spherical, inelastic, and smooth, and the flow is turbulent and incompressible. The cohesion between ice particles is also not considered, since it is of more importance when particle agglomeration exists in laminar flow conditions.

3.1 Continuity equation

The solid and liquid phase continuity equations are mathematical formulas that express the conservation of mass for each individual phase in a multiphase system. For the solid phase, the continuity equation takes into account the conservation of mass within the solid material. It factors in the deformation and movement of the solid particles, giving information on the distribution and density variation within the solid phase. Conversely, the liquid phase continuity equation is concerned with the conservation of mass in the liquid part of the system. The equation considers the flow and redistribution of liquid, including changes in liquid density and velocity.

Continuity equations for phases i.e. solid and liquid are expressed in Eq. (1). and Eq. (2), respectively [39].

$$\frac{\partial}{\partial t}\left(\Phi_l \rho_l\right) + \nabla \cdot \left(\Phi_l \rho_l \vec{u}_l\right) = 0 \tag{1}$$

$$\frac{\partial}{\partial t}\left(\Phi_s \rho_s\right) + \nabla \cdot \left(\Phi_s \rho_s \vec{u}_s\right) = 0 \tag{2}$$

The subscript l signifies liquid while, s denotes solid phase. The local volume fraction for phases is related as follows:

$$\Phi_l + \Phi_s = 1 \tag{3}$$

3.2 Momentum equation

Similar to continuity equation, momentum equation was also solved for both the phases. The momentum equation, when solved for both solid and liquid phases in a multiphase system, involves extending the principles of classical mechanics to describe the motion and interactions of particles within each phase. In addition to it, interphase momentum transfer has also been expressed as a result of various forces applied on that phase. Equation (4) and (6) are momentum equation for liquid phase and solid phase, respectively [39].

$$\frac{\partial}{\partial t}\left(\Phi_l \rho_l \vec{u}_l\right) + \nabla \cdot \left(\Phi_l \rho_l \vec{u}_l \vec{u}_l\right) = -\Phi_l \nabla P + \nabla \tau_l + \Phi_l \rho_l \vec{g} + \vec{R}_{sl} \tag{4}$$

$$\tau_l = \Phi_l \mu_l \left(\nabla \vec{u}_l + \nabla \vec{u}_l^T \right) + \Phi_l \left(\lambda_l - \frac{2}{3} \mu_l \right) (\nabla \vec{u}_l) \bar{I} \tag{5}$$

$$\frac{\partial}{\partial t} \left(\Phi_s \rho_s \vec{u}_s \right) + \nabla \cdot \left(\Phi_s \rho_s \vec{u}_s \vec{u}_s \right) = -\Phi_s \nabla P + \nabla \tau_s + \Phi_s \rho_s \vec{g} - \nabla P_s + \vec{R}_{ls} \tag{6}$$

$$\tau_s = \Phi_s \mu_s \left(\nabla \vec{u}_s + \nabla \vec{u}_s{}^T \right) + \Phi_s \left(\lambda_s - \frac{2}{3} \mu_s \right) (\nabla \vec{u}_s) \bar{I} \tag{7}$$

3.3 Interfacial forces

In the realm of multi-phase flow, various interfacial forces come into play, including virtual mass force, drag force, lift force, and turbulent dispersion force. Specifically, in the context of ice slurry flow, the virtual force is deemed insignificant and can thus be disregarded. This is primarily due to the relatively small density difference between the solid phase (ice) and the liquid phase (water), falling within the range of 10% [21]. The drag force employed in the current study for two-phase flow is derived from Gidaspow [40].

$$\vec{F}_{D,sl} = K_{sl} \left(\vec{u}_s - \vec{u}_l \right) \tag{8}$$

$$\vec{F}_{D,ls} = K_{ls} \left(\vec{u}_l - \vec{u}_s \right) \tag{9}$$

Where $K_{ls}(=K_{sl})$ is interphase momentum exchange coefficients and for $\Phi_l > 0.8$, K_{sl} is expressed as [40],

$$K_{sl} = \frac{3}{4} C_D \frac{\Phi_s \Phi_l \rho_l \left| \vec{u}_s - \vec{u}_l \right|}{d_s} \Phi_l^{-2.65} \tag{10}$$

Where, C_D is the drag force coefficient

$$C_D = \frac{24}{\Phi_l \mathrm{Re}_s} \left[1 + 0.15 \left(\Phi_l \mathrm{Re}_s \right)^{0.687} \right] \tag{11}$$

While when $\Phi_l \leq 0.8$, K_{sl} is expressed as

$$K_{sl} = \frac{150 \Phi_s^2 \mu_l}{\Phi_l d_s^2} + \frac{1.75 \Phi_s \rho_l \left| \vec{u}_l - \vec{u}_s \right|}{d_s} \Phi_l^{-2.65} \tag{12}$$

The lift force for the flow is evaluated by

$$\vec{F}_{lft,sl} = C_L \rho_l \Phi_s \left(\vec{u}_l - \vec{u}_s \right) \times \nabla \vec{u}_l \tag{13}$$

$$\vec{F}_{lft,sl} = -\vec{F}_{lft,ls} \tag{14}$$

The force (turbulent dispersion), which represents interphase turbulent momentum transfer, has been formulated by Burns et al. [41]. In laminar fluid flow conditions, its value is zero. In the context of two-phase flow, the force (turbulent dispersion) plays a critical part in dispersing solid particles away from regions with higher concentration, thereby contributing to improved uniformity in the distribution of solid particles.

$$\vec{F}_{td,s} = C_{TD} K_{sl} \frac{\mu_{t,i}}{\sigma_{sl}} \left(\frac{\nabla \Phi_s}{\Phi_s} - \frac{\nabla \Phi_l}{\Phi_l} \right) \tag{15}$$

Where, C_{TD} is coefficient of turbulent dispersion force and has value of 1, while dispersion Prandtl number (σ_{sl}) has the value 0.9.

3.2 Bulk viscosity and shear viscosity

Bulk viscosity, is the resistance of solid particles i.e. ice for compression and expansion and is expressed as [42]

$$\lambda_s = \frac{4}{3} \Phi_s \rho_s d_s g_{o,ss} \left(1 + e_{ss}\right) \left(\frac{\theta_s}{\pi} \right)^{0.5} \tag{16}$$

While the solid shear viscosity (μ_s) is expressed in equation (17). Another viscosity i.e. frictional viscosity plays a significant role when particle concentration is above the frictional limit of concentration [39]. Expressions for collision and kinetic viscosity are given in Eq. (18) and Eq. (19), respectively [34].

$$\mu_s = \mu_{\text{col}} + \mu_{\text{kin}} \tag{17}$$

$$\mu_{\text{col}} = \frac{4}{5} \Phi_s \rho_s d_s g_{o,ss} \left(1 + e_{ss}\right) \left(\frac{\theta_s}{\pi} \right)^{0.5} \tag{18}$$

$$\mu_{\text{kin}} = \frac{\Phi_s \rho_s d_s \sqrt{\pi \theta_s}}{6 \left(3 - e_{ss}\right)} \left[1 + \frac{2}{5} \left(1 + e_{ss}\right) \left(3 e_{ss} - 1\right) \Phi_s g_{o,ss} \right] \tag{19}$$

$g_{o,ss}$ has been defined by Lun et al. [42] as:

$$g_{o,ss} = \left[1 - \left(\frac{\Phi_s}{\Phi_{s,\,\max}} ()^{\frac{1}{3}} \right) [] \right]^{-1} \tag{20}$$

3.3 Granular flow kinetics

The dynamics of two-phase flow, involving solid-liquid interactions, play a pivotal role in various industries such as mining, food processing, and sediment transportation. Instances where particle interactions significantly influence

flow behavior are termed granular flow [43], [44]. Due to the densely packed nature of solid-liquid flow, ice slurry flow can be categorized as a granular flow, exhibiting distinct flow patterns compared to conventional single-phase fluid flow. Granular flow encompasses three distinct regimes: elastic, plastic, and viscous. The elastic regime is characterized by stagnancy, where stress is dependent on strain, allowing for the application of elasticity in flow modeling. The plastic regime involves slower flow velocities with strain rates independent of stress, making theories of soil mechanics suitable for modeling this region. The viscous regime, akin to the plastic regime but with rapid particle flow, is of particular concern in the current study on ice slurry flow.

Within the viscous regime of granular flow, particles exhibit random motion due to interactions with the pipe wall. This interaction leads to material dilation, causing the granular material to behave like gas molecules. Flow modeling in this regime is achieved through kinetic theory, wherein the fluctuating velocity and energy of particles are expressed in terms of granular temperature (θ_s).

$$\theta_s = \frac{1}{3}\overline{u_s' u_s'} \tag{21}$$

The θ_s can be determined from fluctuating energy balance equation, which is expressed in Eq. (22).

$$\frac{3}{2}\left[\frac{\partial}{\partial t}\left(\Phi_s \rho_s \theta_s\right) + \nabla \cdot \left(\Phi_s \rho_s \vec{v}_s \theta_s\right)\right] = \left(-P_s \bar{I} + \tau_s\right) : \nabla \vec{v}_s + \nabla \cdot \left(K_{\theta_s} \nabla \theta_s\right) + \phi_{ls} - \gamma_{\theta_s} \tag{22}$$

P_s is solid pressure and its expression is:

$$P_s = \Phi_s \rho_s \theta_s + 2\rho_s \left(1 + e_{ss}\right) \Phi_s^2 \cdot g_{o,ss} \theta_s \tag{23}$$

3.4 Turbulent equations

To simulate turbulence in two-phase (solid-liquid) flow, various models such as the mixture k-ε model, dispersed model, and per-phase model can be employed. The choice of model depends on the specific flow type or application. Firstly, the mixture k-ε model is suitable for more heterogeneous solid-liquid flow, serving as an extension of the single-phase k-ε turbulence model and particularly well-suited for problems with stratified flow. Secondly, the dispersed model is used when particle concentration is below 10%. Finally, the k-ε per-phase model is the most complicated of the three, with individual calculations for turbulence variables (k and ε) for each phase. This model is more generalized and can be used for any kind of two-phase flow. For the current investigation on ice slurry flow, the turbulence modeling methodology employed is the per-phase k-ε method, as per the methodology applied in Zhang and Jiang [13].

The numerical simulation of ice slurry flow in a bend pipe might have some restraints. Multi-phase flow in bends, due to its intricacy, constitutes complex interactions among phases that can be over-simplified in a model. Some real-world phenomenology such as turbulence, particle-particle, and wall effect may not be accurately captured. The study focuses on concentration and pressure drop but does not mention the impact of thermal effects, such as melting or heat transfer, which can significantly influence ice slurry behavior in practical applications. The model assumes a uniform initial distribution of ice particles, which can differ from real-world conditions where particle aggregation or uneven distribution might occur. Range of concentrations and particle size considered may not encompass all practical scenarios, and different concentrations or particle sizes could yield different results.

4 Meshing and validation

Table 2 and 3 shows the value of optimum elements after performing grid independence test and boundary conditions respectively for the present problem. Multi zone mesh has been generated using FLUENT meshing tool in the 180° bend pipes (shown in Figure 2). The mesh independent tests for both the bend radius ratio also have been performed

and the optimum mesh sizes are 474,195 and 530,262 for R/r ratio 2.98 and 5.60 respectively. Apart from the optimum mesh size, the solution (convergence) of any CFD problem depends upon the quality of the mesh which can be determined by the different mesh parameters viz. element quality, orthogonal quality, aspect ratio and element volume. For the commercial code FLUENT as a solver, the minimum element quality should be greater than 0.2. The critical mesh quality parameters have also been summarized for the different bend radius ratio pipes in Table 2.

Table 2:

Optimum mesh size for different geometries.

	Geometry	Minimum element quality	Minimum orthogonal quality	Maximum aspect ratio	Optimum number of elements
180° U-shaped pipe	($R/r = 2.98$)	0.35	0.793	4.864	474,195
	($R/r = 5.60$)	0.304	0.63	6.106	530,262

Table 3:

Boundary conditions opted in present work.

Boundary	Boundary condition	Description
Inlet	Velocity inlet	Liquid phase velocity = solid phase velocity
Outlet	Pressure outlet	For mixture: Atmospheric pressure
Wall	Wall	For liquid: No slip For solid: Partial slip

Figure 2:

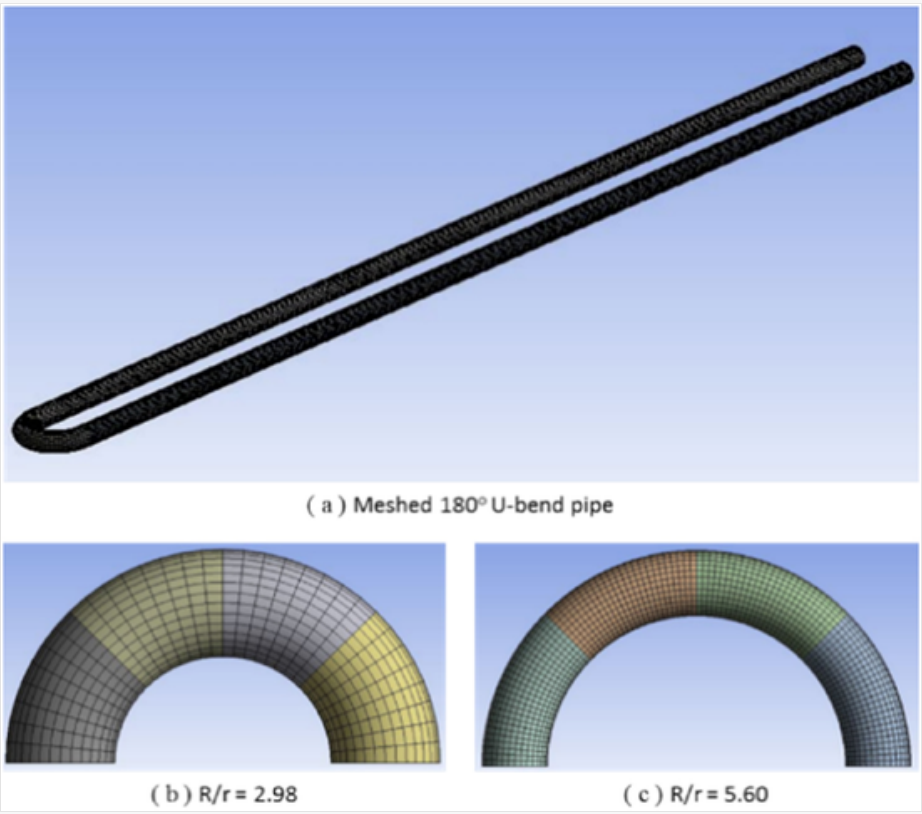

Meshed 180° bend pipes.

This section presents a thorough overview of the specific boundary conditions implemented for both phases in the current simulation. Each phase is assigned distinct boundary conditions. A uniform and steady velocity for both liquid and solid phases, along with an unyielding ice concentration equally distributed within the solid phase, is given at the inlet of the pipe. As the fluid flows through bifurcating sections toward outlets, a pressure outlet condition is applied to maintain atmospheric pressure. In a quest to mimic adiabatic ice slurry flow, the wall of the pipe is set to be adiabatic, thus inhibiting any possible heat transfer. In addition to this, in a bid to simulate the system realistically, the wall is subject to a no-slip condition, which forces the liquid phase to follow closely the wall surface without slipping. These specific conditions and limitations are part of the overall description of the ice slurry dynamics in the pipe system, accounting for significant features of velocity, concentration, and thermal characteristics. For wall-solid phase interactions, conditions proposed by Johnson and Jackson [45] are utilized. This involves the application of a partial slip condition for the solid phase, with a coefficient of restitution for particle-wall collisions (ε) set at 0.95 and a specularity coefficient (σ) at 0.02. Moreover, the particle-wall collision also affects the shear stress and fluctuation energy flux, calculated using the expression provided by Jin et al. [46].

The ice slurry consists of ethanol as a freezing point depressant with a concentration of 10 %. The characterization of the ice (solid phase) within the system involves assigning a density of 915 kg/m^3. On the other hand, the liquid phase introduces complexity, as both density and viscosity exhibit dependence on the ice concentration. Across the range of ice concentrations from 10 % to 30 %, the density of the liquid phase fluctuates between 983.9 kg/m^3 and 981.3 kg/m^3, while the viscosity undergoes changes from 0.00458 m-Pa to 0.00609 m-Pa. This nuanced approach accounts for the dynamic nature of the fluid properties based on varying ice concentrations. The entire computational domain, crucial for accurate simulations, is discretized using structured grids comprised of hexahedral volume elements. One key advantage of structured meshing is its ability to align with the geometry of the simulation domain, resulting in a grid composed of structured elements, typically quadrilaterals or hexahedra. This structured nature simplifies the numerical solution of partial differential equations governing fluid flow, heat transfer, or other physical phenomena, as it allows for a more straightforward representation of the governing equations on the mesh. This discretization is facilitated through the ICEM module, an integral component of the ANSYS commercial code. Such meticulous detailing of material properties and computational grid construction is essential for capturing the intricacies of the ice slurry system,

ensuring a comprehensive and accurate representation of the fluid dynamics and thermal behavior. Various researcher has opted commercial code for similar problem simulation.

The current model's validation was conducted using experimental data from Kaushal et al. [22]. To achieve this, a comparable geometry was replicated and simulated under identical operating conditions. The validation specifically focused on the 90° elbow bend pipe geometry studied by Kaushal et al. [22], and the agreement between the normalized pressure drop along the pipe length, as depicted in Figure 2(b), demonstrates that the predicted values from the present numerical approach closely align with the findings of the previous study. The result comparison with experimental [5] has been shown in Figure 3, the variation in experimental and simulation values is within 10 %. The present work, which deals with ice particles, differs from Kaushal et al. [22], which focuses on silica sand particles. However, as there is no melting involved, we can say that density difference may be the reason for 10 % deviation. The current model has also been validated for heterogeneous ice slurry flow in both horizontal and vertical pipes. Figure 3(b) illustrates a comparison of the velocity profiles for ice slurry flow with experimental data from Vuarnoz et al. [47]. The validation was conducted for a 10.3 % ethanol-based ice slurry containing particles with a diameter of 0.1 mm, flowing through a horizontal pipe with a diameter of 23 mm and a length of 2 m. The velocity profile is shown for an initial velocity of 1.25 m/s and an initial particle concentration of 16 % along the vertical line at the center of the pipe outlet. Since experimental data for the ice particle concentration profile is unavailable, validation was performed using sand-water slurry flow data from a 10 m long horizontal pipe, as reported by Gillies and Shook [48]. Figure 3(c) compares the numerical and experimental results for the concentration profile, considering an inlet velocity of 3 m/s, an initial sand particle concentration of 19 %, and a particle diameter of 0.09 mm. The concentration profile is depicted along a vertical line at the center of the cross-section, located 8.5 m from the pipe inlet.

Figure 3:

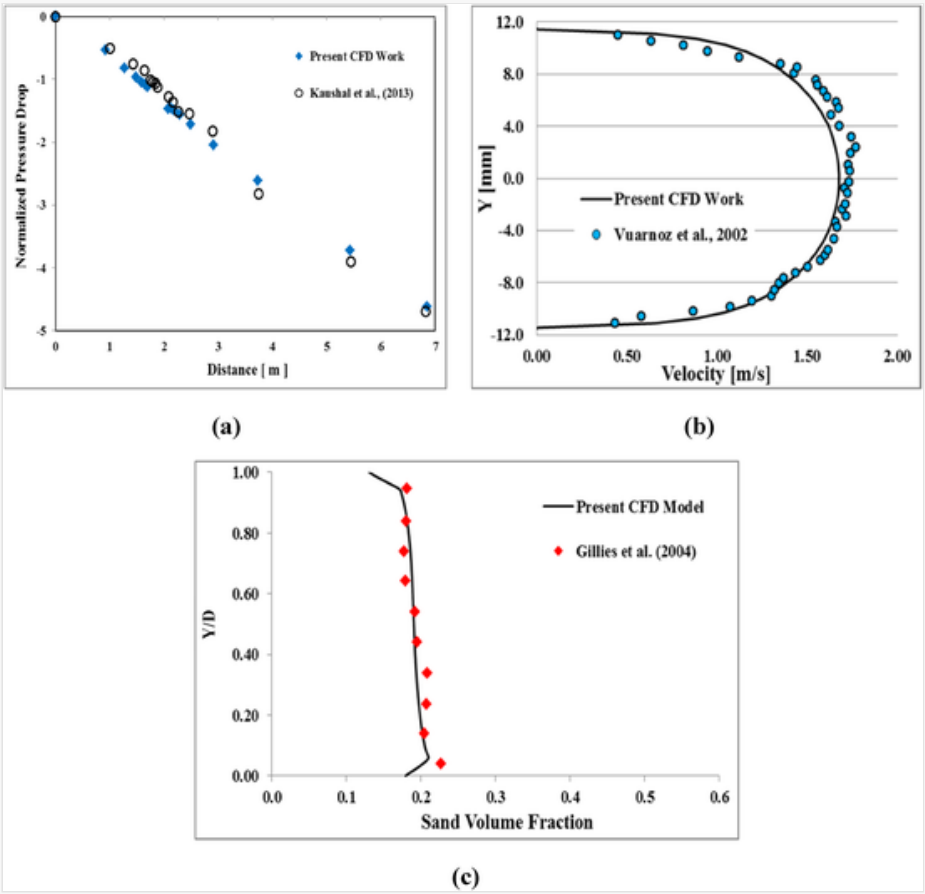

Fig.3. Variation in experimental and simulation values, (a) Comparison between the present results and experimental data [22], (b) comparison of velocity profile in horizontal pipe with Vuarnoz et al. [47] (c) comparison of sand particles concentration profile in horizontal pipe Gillies and Shook [48].

Q6

5 Results and discussion

CFD investigation of flow has been done for ice concentrations of 10, 20 and 30 % by volume at 1 m/s to 3 m/s velocities, and particles of 0.25 mm and 0.40 mm diameters. The results of the investigations have been discussed in the following section.

5.1 Velocity at different bend angles

For the $R/r = 2.98$ pipe, contours and vector plots of the velocity has been shown in Figures 4 and 5 respectively. The results are presented for the 10 % C_2H_5OH based IS with 0.25 mm size particles at the velocity of 1 m/s and concentration of 10 %.

Figure 4:

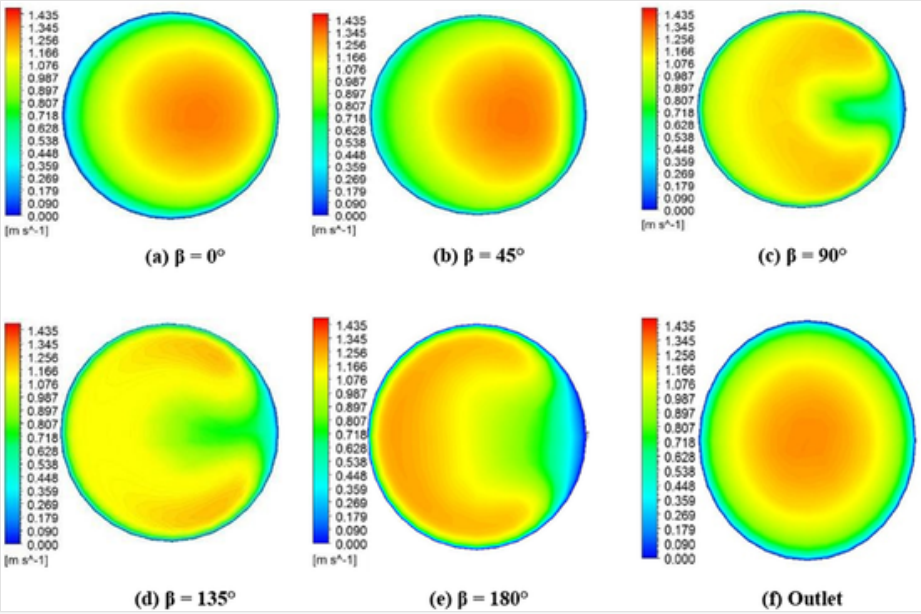

Contours of velocity at different bend angles in U-bend pipe.

Figure 5:

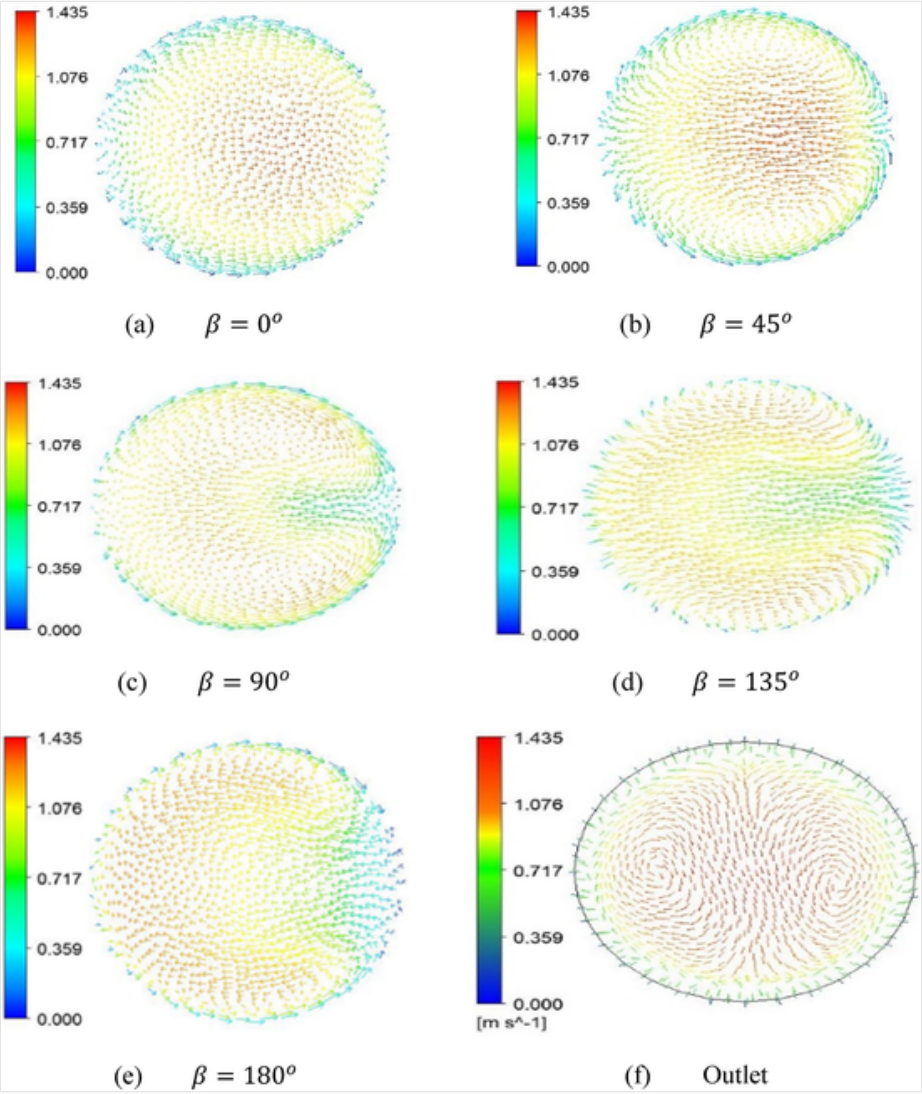

Velocity vector at different bend angles in U-bend pipe.

The plots illustrate the cross-sectional views of a U-bend pipe at various bend angles (β = 0°, 90°, 135°, and 180°), focusing on the velocity distribution. In Figures 4(a) and 5(a), which depict the starting point of the bend (β = 0°), the contour plot and vector plot respectively reveal that the velocity is highest towards the inner side of the bend. This phenomenon is attributable to the smaller curvature of the bend, which directs fluid particles inward.

As the bend progresses, secondary flow effects become apparent: velocity decreases on the inner side and increases on the outer side, as depicted in Figure 4(b)–(e). The vector plots presented in Figure 5(b)–(e) provide visual confirmation of this observation. These plots illustrate the movement of particles in an outward direction, which can be attributed to the influence of centrifugal forces or the presence of radial pressure gradients. As these forces act on the particles, they experience a displacement away from the central region, further validating the observed motion patterns. The graphical representation effectively highlights the underlying physical mechanisms responsible for this outward movement.

Simultaneously, fluid flows from the outer bend side towards the inner bend side along the pipe wall to maintain continuous flow. Upon exiting the bend section, the flow redistributes once more. At the outlet (Figure 4(f)), maximum velocity occurs at the center of the pipe, tapering to zero towards the walls. Figure 5(f) highlights two prominent vortices of recirculation observed at the pipe's center, indicative of complex flow dynamics and vortical structures

within the pipe. Thus, the sequence of plots provides a comprehensive visualization of how velocity profiles evolve through the U-bend pipe, influenced by curvature, secondary flows, and centrifugal effects, ultimately affecting flow distribution and vorticity patterns within the pipe's cross-sections.

5.2 Particle distribution at different bend angles

Figures 6–8 present contour plots illustrating the instantaneous solid fraction (ISF) within the bend section ($\beta = 0°$, 45°, 90°, 135°, and 180°) and at the outlet of a U-bend pipe with a radius-to-diameter ratio (R/r) of 2.98.

Figure 6:

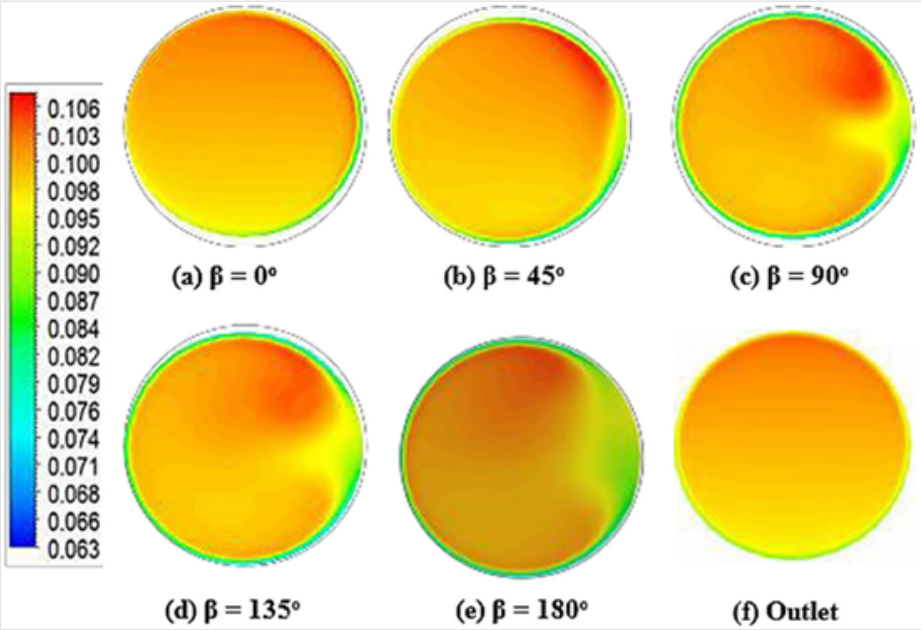

Contours of particle concentration at different bend angle in U-bend pipe at $V = 1$ m/s.

Figure 7:

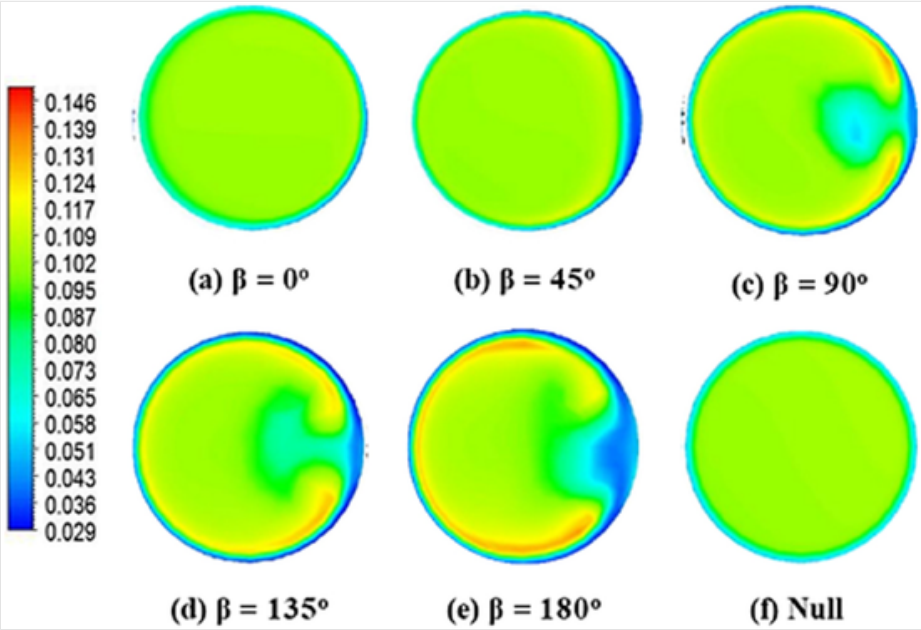

Particle concentration contours at different bend angle in U-bend pipe at $V = 3$ m/s.

Figure 8:

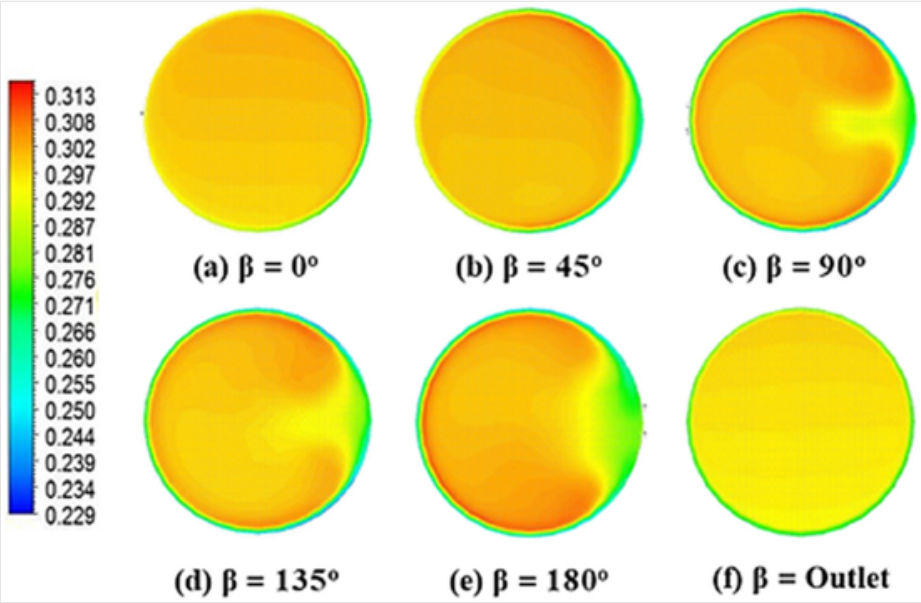

Particle concentration contour at different bend angle in U-bend pipe at IPC = 30 %.

In Figure 6, the contours depict the distribution of a 10% ethanol-based suspension with 0.25 mm particle size at a velocity of 1 m/s. In Figure 6(a), at the beginning of the bend section, particles are uniformly distributed due to high velocity. However, concentration is slightly elevated near the inner bend side due to the bend's curvature. As the fluid moves through the curved section of a conduit or channel, it experiences centrifugal forces due to the change in direction. These forces, also referred to as radial pressure gradients, push the suspended particles outward toward the outer edge of the bend. As a result, the distribution of particles within the fluid becomes uneven, with a higher concentration accumulating near the outer curve while the inner bend retains a relatively lower concentration. This phenomenon disrupts the uniformity of the particle dispersion within the flow, creating a gradient in particle concentration across the bend. While, at the outlet of the pipe, Figure 6 shows a more uniform concentration distribution due to flow redistribution.

Figure 7 illustrates the contours for the same suspension at a higher velocity of 3 m/s. Comparing Figure 7 with Figure 8, it is evident that the concentration distribution is more uniform at higher velocities. However, beyond $\beta = 45°$, towards the inner side of the bend, concentration is significantly lower. This discrepancy arises because secondary flow effects become more pronounced at higher velocities, influencing particle distribution and resulting in less uniform concentration profiles in the inner bend regions. These figures provide detailed insights into how velocity, particle size, and suspension concentration interact within the U-bend pipe, highlighting the influence of bend curvature and secondary flows on particle distribution and concentration uniformity throughout the bend section and at the outlet.

Figure 8 shows the contours for 10 % ethanol based IS with 0.25 mm particle size at a velocity of 1 m/s and concentration of 30%. At higher concentration, the collisions between particles are more frequents due to which the

concentration distribution in the bend section is more uniform with high concentration. However, concentration distribution is more disturbed in comparison to lower concentration beyond the $\beta = 45°$ due to secondary flow.

Figure 9 shows the contours of concentration for the ISF at different bend angles ($\beta = 0°, 45°, 90°, 135°$& $180°$) of the bend section and the outlet of the U-bend pipe with bend radius ratio of 5.6. The figure shows the contour of concentration for 10 % ethanol based IS with 0.25 mm particle size at a velocity of 1 m/s and concentration of 10 %. The contour (a) shows the concentration at the starting of bend section. From the comparison of Figures 6 and 9 of the concentration distribution between the U-bend pipe with R/r ratio 2.98 & 5.60, it can be observed that concentration distribution is almost same for both R/r ratios however, the concentration distribution near to inner side of the bend is less affected for higher R/r ratio. Apart from that results are same as for R/r ratio of 2.98.

Figure 9:

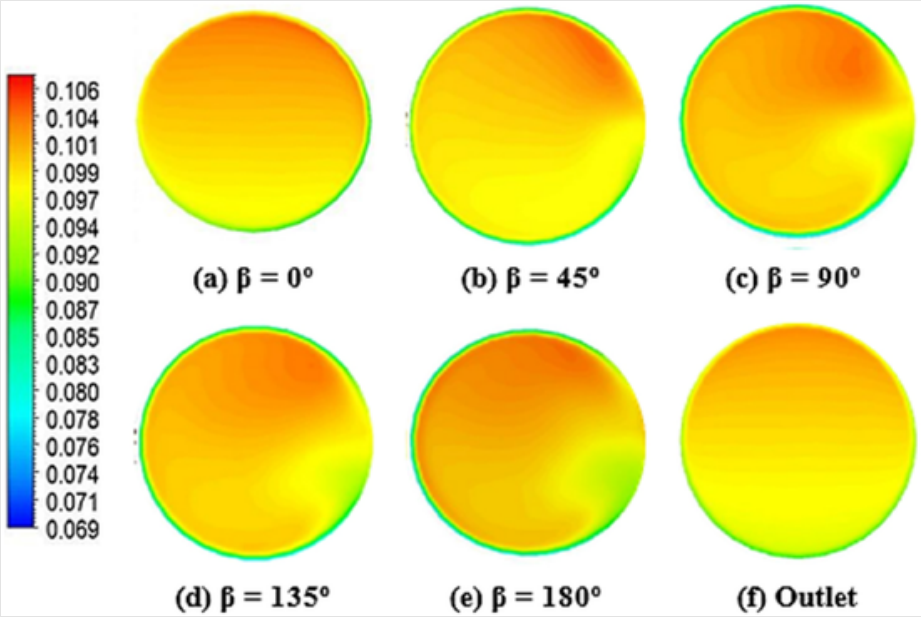

Particle concentration contour at different bend angle for $R/r = 5.6$.

5.3 Pressure drops

The contours of pressure along the length in the U-bend pipe with bend ratios of 2.98 and 5.60, respectively has been shown in Figure 10. The contours have been plotted in the horizontal plane, which lies exactly at the middle of the pipe. Results are shown for velocity of 1 m/s and concentration of 10 %.

Figure 10:

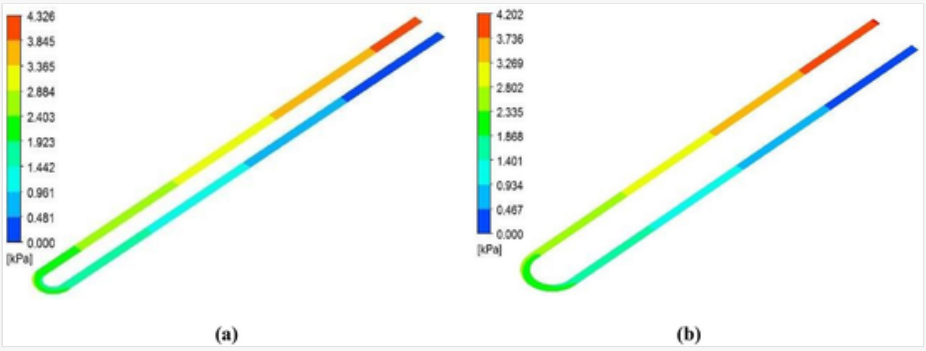

Contours of pressure in the horizontal plane of 180° U-bend pipe (A) bend radius of 2.98 (B) bend radius of 5.60.

From the figures, it is clear that, for upstream and downstream portion pressure varies only in the axial direction. However, in bend section pressure also varies in the radial direction along with axial direction. It can be seen from the comparison between the contours (a) and (b) that the pressure losses are decrease with increase in *R*/*r* ratio.

Figure 11 shows the deviation in pressure drop per unit length with concentration for *R*/*r* ratio of 2.98 and 5.60 in the U-band pipe. The results are shown for the 10% C_2H_5OH based IS with 0.25 mm particles size at velocity of 1 m/s. During the ISF the phase interactions, secondary flow, collision between particles and with wall are responsible for pressure losses. It can be seen that with the increase in concentration the value of pressure losses increases. The pressure drops increase up to 33% with the increase in concentration from 10% to 30% since at higher concentration particles interaction and collision also increases. However, pressure losses decrease with the increase of bend ratio since with the increase in *R*/*r* ratio secondary flow at the bend section becomes weak. The pressure drops decrease by 9% with increase in the bend ratio.

Figure 11:

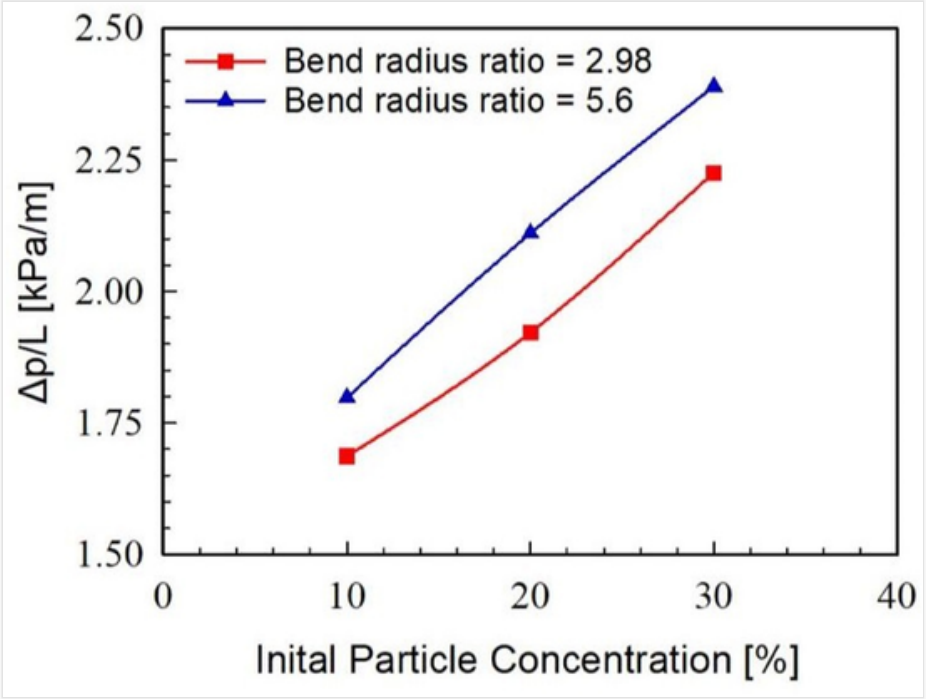

Variation in pressure drop/length with different bend radius ratio.

Variation in pressure drop with velocity at different concentrations in a U-bend pipe. The results are shown for the 10% C_2H_5OH based IS with 0.25 mm particles size for R/r ratio of 2.98. It can be observed from the figure that, the value of pressure losses rises with the velocity and concentration. However, these losses are more with velocity in comparison to concentration as exhibited in the figure 12. (Figure 12).

Q7

Figure alignment: The figure layout displayed in this section is not how it will appear in the final version. As per journal style, figures will only be left aligned. The presentation below is for the sole purpose of providing corrections to the figures. To view the actual presentation of the figures, please click on the PDF located at the top of the page.

Figure 12:

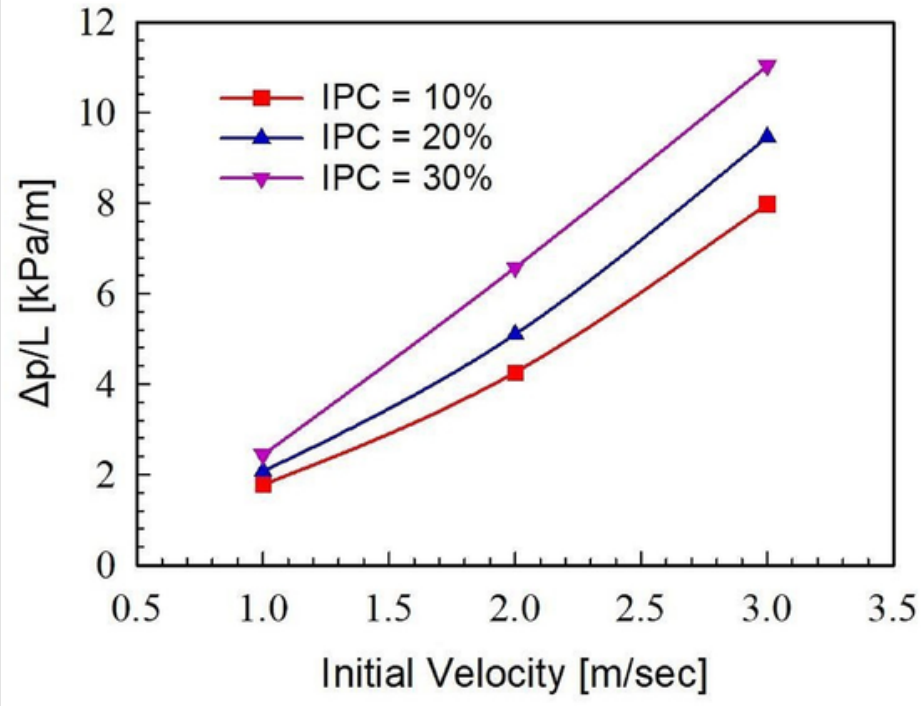

Variation in pressure drop/length with initial velocity and initial particle concentration.

6 Conclusions and future outlook

The numerical simulations of ice slurry flow (ISF) through a 180° U-bend pipe have been performed for two bend ratios, namely R/r = 2.98 and R/r = 5.6. The study of ISF behavior indicates that fluid flow characteristics are highly affected by the occurrence of secondary flow in the curved pipe section. This secondary flow phenomenon is very evident when the bend ratio is lower, meaning that a smaller curvature radius results in a more significant effect on the flow patterns. The distribution of concentration and velocity are significantly affected by this secondary slurry flow. Because of the curved shape of the pipe, ice particles undergo a radial motion, moving from the inner portion of the bend to the outer side. Consequently, the particle concentration is higher on the outer bend and the top part of the pipe, causing an uneven distribution in the bend. Nevertheless, as the slurry moves through the downstream part of the pipe,

the flow redistributes, causing a more uniform velocity and concentration distribution at the exit. In addition, the study identifies the correlation between pressure losses, velocity, and concentration. Pressure losses are seen to increase with rising flow velocity and concentration of slurry. Velocity is more influential in pressure losses than concentration. Further, as the bend ratio increases from 2.98 to 5.60, pressure drop per unit length ($\Delta p/L$) reduces by about 9%, which means a greater bend radius reduces flow resistance in the system.

The scope of future research on the flow of ice slurry in bend sections of a pipeline system can be wide and multi-dimensional. More studies can be carried out to investigate a wider variety of bend geometries, such as various angles (e.g., 45°, 90°) and different radii of curvature. These parameters can be optimized to result in better performance and lower pressure drops in the system. Experiments may be extended to various pipelines with different lengths and diameters. This would facilitate the understanding of scalability of results and their extendability to industrial applications. Research may investigate the use of other additives in the ice slurry for improving flow behavior and thermal properties. Some possible additives may be anti-freeze chemicals, viscosity modifiers, or surfactants. Although CFD simulations are of great help, experimental testing under real conditions is necessary. Evaluation under various environmental conditions and scales can fill the gap between theoretical and practical use. Long-term research into how pipeline materials wear and deteriorate from ice slurry flow, clogging problems, and the maintenance and reliability concerns of such systems. A comprehensive report on the economic advantages and energy efficiency of installing ice slurry systems in numerous industrial processes would assist in pushing its implementation. This includes cost-benefit analyses, return on investment (ROI), and long-term savings. Future research on ice slurry systems can explore their potential applications in industries such as refrigeration, medical cooling, and thermal energy storage, etc.

References

[1] K. Wang, M. Eisele, Y. Hwang, and R. Radermacher, “Review of secondary loop refrigeration systems,” *Int. J. Refrig.*, vol. 33, no. 2, pp. 212–234, 2010. https://doi.org/10.1016/j.ijrefrig.2009.09.018.

[2] A. F. Pachman, et al., “A study of global solar radiations measurement in Java Island, Indonesia,” *Evergreen*, vol. 10, no. 1, pp. 212–218, 2023. https://doi.org/10.5109/6781071.

[3] A. Saito, “Recent advances in research on cold thermal energy storage,” *Int. J. Refrig.*, vol. 25, no. 2, pp. 177–189, 2002. https://doi.org/10.1016/s0140-7007(01)00078-0.

Q10 [4] K. Hayashi and K. E. Kasza, “Ice slurry cooling research: Effects of microscale ice particle characteristics and freezing-point-depressant additives on ice slurry fluidity/Discussion,” *ASHRAE Transactions*, vol. 107, p. 346, 2001.

[5] B. Niezgoda-Zelasko and J. Zelasko, “Melting of ice slurry under forced convective conditions in tubes,” *Exp. Therm. Fluid Sci.*, vol. 32, no. 8, pp. 1597–1608, 2008.

[6] D. W. Lee, E. S. Yoon, M. C. Joo, and A. Sharma, “Heat transfer characteristics of the ice slurry at melting process in a tube flow,” *Int. J. Refrig.*, vol. 29, no. 3, pp. 451–455, 2006. https://doi.org/10.1016/j.ijrefrig.2005.10.003.

[7] J. Wang, S. Wang, T. Zhang, and F. Battaglia, “Mathematical and experimental investigation on pressure drop of heterogeneous ice slurry flow in horizontal pipes,” *Int. J. Heat Mass Transfer*, vol. 108, pp. 2381–2392, 2017. https://doi.org/10.1016/j.ijheatmasstransfer.2017.01.083.

[8] G. V. Messa, M. Malin, and S. Malavasi, “Numerical prediction of fully-suspended slurry flow in horizontal pipes,” *Powder Technol.*, vol. 256, pp. 61–70, 2014. https://doi.org/10.1016/j.powtec.2014.02.005.

[9] L. Cai, S. Mi, C. Luo, and Z. Liu, "Numerical investigation on heat and mass transfer characteristics of ice slurry in pulsating flow," *Int. J. Heat Mass Transfer*, vol. 189, 2022, Art no. 122722. https://doi.org/10.1016/j.ijheatmasstransfer.2022.122722.

[10] M. Grozdek, R. Khodabandeh, and P. Lundqvist, "Experimental investigation of ice slurry flow pressure drop in horizontal tubes," *Exp. Therm. Fluid Sci.*, vol. 33, no. 2, pp. 357–370, 2009. https://doi.org/10.1016/j.expthermflusci.2008.10.003.

[11] M. M. Kamra and C. Hu, "Implementation of unstructured multi-dimensional THINC for practical multi-phase flow simulations," *Evergreen*, vol. 4, no. 1, pp. 52–57, 2017. https://doi.org/10.5109/1808453.

[12] M. Kumar Gopaliya and D. R. Kaushal, "Modeling of sand-water slurry flow through horizontal pipe using CFD," *J. Hydrol. Hydromech.*, vol. 64, no. 3, pp. 261–272, 2016. https://doi.org/10.1515/johh-2016-0027.

[13] P. Zhang and Y. Y. Jiang, "Forced convective heat transfer of slush nitrogen in a horizontal pipe," *Int. J. Heat Mass Transfer*, vol. 71, pp. 158–171, 2014. https://doi.org/10.1016/j.ijheatmasstransfer.2013.11.078.

[14] B. B. Nayak and D. Chatterjee, "Numerical investigation of convective heat transfer in pipeline flow of multi-sized mono dispersed fly ash-water slurry," *Int. J. Heat Mass Transfer*, vol. 108, pp. 1802–1818, 2017. https://doi.org/10.1016/j.ijheatmasstransfer.2017.01.057.

[15] M. Easa and M. Barigou, "CFD investigation of the transport of coarse solids in laminar power law fluids," *Chem. Eng. Sci.*, vol. 64, no. 2, pp. 322–333, 2009.

[16] Y. Y. Jiang and P. Zhang, "Numerical investigation of slush nitrogen flow in a horizontal pipe," *Chem. Eng. Sci.*, vol. 73, no. 7, pp. 169–180, 2012. https://doi.org/10.1016/j.ces.2012.01.027.

[17] K. Ekambara, R. S. Sanders, K. Nandakumar, and J. H. Masliyah, "Hydrodynamicsimulation of horizontal slurry pipeline flow using ANSYS-CFX," *Ind. Eng. Chem. Res.*, vol. 48, no. 17, pp. 8159–8171, 2009. https://doi.org/10.1021/ie801505z.

[18] B. Niezgoda-Zelasko and W. Zalewski, "Momentum transfer of ice slurry flows in tubes, modeling," *Int. J. Refrig.*, vol. 29, no. 3, pp. 429–436, 2006. https://doi.org/10.1016/j.ijrefrig.2005.09.006.

[19] J. H. Wang, S. G. Wang, T. F. Zhang, and Y. T. Liang, "Numerical investigation of iceslurry isothermal flow in various pipes," *Int. J. Refrig.*, vol. 36, no. 1, pp. 70–80, 2013. https://doi.org/10.1016/j.ijrefrig.2012.08.007.

[20] Q. Tian, G. He, H. Wang, and D. Cai, "Simulation on transportation safety of ice slurry in ice cooling system of buildings," *Energy Build.*, vol. 72, pp. 262–270, 2014. https://doi.org/10.1016/j.enbuild.2013.12.033.

Q11 [21] P. Zhang and X. J. Shi, "Thermo-fluidic characteristics of ice slurry in horizontal circular pipes," *Int. J. Heat Mass Transfer*, vol. 89, pp. 950–963, 2015. https://doi.org/10.1016/j.ijheatmasstransfer.2015.06.008.

[22] D. R. Kaushal, A. Kumar, Y. Tomita, S. Kuchii, and H. Tsukamoto, "Flow of mono-dispersed particles through horizontal bend," *Int. J. Multiphase Flow*, vol. 52, pp. 71–91, 2013. https://doi.org/10.1016/j.ijmultiphaseflow.2012.12.009.

[23] R. Giguère, L. Fradette, D. Mignon, and P. A. Tanguy, "Analysis of slurry flow regimes downstream of a pipe bend," *Chem. Eng. Res. Des.*, vol. 87, no. 7, pp. 943–950, 2009.

https://doi.org/10.1016/j.cherd.2009.01.005.

[24] A. Kamyar, S. M. Aminossadati, C. R. Leonardi, A. P. Sasmito, and S. Poncet, “Flow characterisation of monopropylene glycol ice slurry through a horizontal U-bend: A numerical approach,” *Eur. J. Mech./B Fluid*, vol. 82, pp. 93–105, 2020. https://doi.org/10.1016/j.euromechflu.2020.03.004.

[25] G. Vittorio Messa and S. Malavasi, “Numerical prediction of particle distribution of solid-liquid slurries in straight pipes and bends,” *Eng. Appl. Comput. Fluid Mech.*, vol. 8, no. 3, pp. 356–372, 2014. https://doi.org/10.1080/19942060.2014.11015521.

[26] X. J. Shi and P. Zhang, “Two-phase flow and heat transfer characteristics of tetra-n-butyl ammonium bromide clathrate hydrate slurry in horizontal 90° elbow pipe and U-pipe,” *Int. J. Heat Mass Transfer*, vol. 97, pp. 364–378, 2016. https://doi.org/10.1016/j.ijheatmasstransfer.2016.02.007.

[27] L. Cai, et al., “Investigation on flow characteristics of ice slurry in horizontal 90° elbow pipe by a CFD-PBM coupled model,” *Adv. Powder Technol.*, vol. 30, pp. 2299–2310, 2019. https://doi.org/10.1016/j.apt.2019.07.010.

[28] K. Ma, Z. Liu, Y. Tang, X. Liu, Y. Yang, and S. Yang, “Numerical investigation on ice slurry flow in horizontal elbow pipes,” *Therm. Sci. Eng. Prog.*, vol. 27, 2022, Art no. 10083. https://doi.org/10.1016/j.tsep.2021.101083.

[29] L. Cai, S. Mi, C. Luo, and Z. Liu, “Numerical investigation of hydraulic and heat transfer characteristics of two-phase ice slurry in helically coiled tubes,” *Energy Build.*, vol. 256, 2022, Art no. 111773. https://doi.org/10.1016/j.enbuild.2021.111773.

[30] O. Parkash, A. Kumar, and B. Sikarwar, “CFD modeling of slurry pipeline at different Prandtl numbers,” *J. Therm. Eng.*, vol. 7, no. 4, pp. 951–969, 2021. https://doi.org/10.18186/thermal.930932.

[31] T. Joshi, O. Parkash, and G. Krishan, “Slurry flow characteristics through a horizontal pipeline at different Prandtl number,” *Powder Technol.*, vol. 413, 2023, Art no. 118008. https://doi.org/10.1016/j.powtec.2022.118008.

[32] T. Joshi, O. Parkash, and G. Krishan, “CFD modeling for slurry flow through a horizontal pipe bend at different Prandtl number,” *Int. J. Hydrogen Energy*, vol. 47, no. 56, pp. 23731–23750, 2022. https://doi.org/10.1016/j.ijhydene.2022.05.201.

[33] T. Joshi, O. Parkash, and G. Krishan, “Estimation of energy consumption and transportation characteristics for slurry flow through a horizontal straight pipe using computational fluid dynamics,” *Phys. Fluids*, vol. 35, no. 5, 2023. https://doi.org/10.1063/5.0146534.

[34] O. P. Verma, A. A. Kumar, and B. S. Sikarwar, “Numerical simulation and comparative analysis of pressure drop estimation in horizontal and vertical slurry pipeline,” *J. Mech. Eng. Sci.*, vol. 14, no. 2, pp. 6610–6624, 2020. https://doi.org/10.15282/jmes.14.2.2020.06.0518.

[35] O. Parkash, A. Kumar, and B. S. Sikarwar, “Computational erosion wear model validation of particulate flow through mitre pipe bend,” *Arabian J. Sci. Eng.*, vol. 46, pp. 12373–12390, 2021. https://doi.org/10.1007/s13369-021-05931-x.

[36] T. Joshi, O. Parkash, G. Krishan, and A. A. Murthy, “Numerical investigation of Bi-model slurry transportation through horizontal pipe bend,” *Powder Technol.*, vol. 418, 2023, Art no. 118284. https://doi.org/10.1016/j.powtec.2023.118284.

[37]

M. Rezaei and H. A. Pakravan, “Thermo-fluidic characteristics of ice slurry flows in U-bend pipes for cold thermal energy storage,” *J. Energy Storage*, vol. 57, 2023, Art no. 106224. https://doi.org/10.1016/j.est.2022.106224.

[38] T. Joshi, O. Parkash, R. K. B. Gallegos, and G. Krishan, “Computational investigation of transportation and thermal characteristics in a bi-modal slurry flow through a horizontally placed pipe bend,” *Powder Technol.*, vol. 442, 2024, Art no. 119879. https://doi.org/10.1016/j.powtec.2024.119879.

[39] K. Rawat, P. Bhandari, V. S. Bisht, T. Alam, and M. I. H. Siddiqui, “Numerical investigation of adiabatic ice slurry flow through a horizontal T–shaped pipe,” *Fluid Dynam.*, vol. 59, pp. 344–362, 2024. https://doi.org/10.1134/s0015462823602309.

Q12 [40] D. Gidaspow, *Multiphase Flow and Fluidization: Continuum and Kinetic Theory Descriptions*, Academic Press, 1994.

[41] A. D. Burns, T. Frank, I. Hamill, and J. M. Shi, “The Favre averaged drag model for turbulent dispersion in Eulerian multi-phase flows,” in *5th International Conference on Multiphase Flow*, vol. 4, ICMF, 2004, pp. 1–17.

[42] C. K. K. Lun, S. B. Savage, D. J. Jeffrey, and N. Chepurniy, “Kinetic theories for granular flow: Inelastic particles in Couette flow and slightly inelastic particles in a general flow field,” *J. Fluid Mech.*, vol. 140, pp. 223–256, 1984. https://doi.org/10.1017/s0022112084000586.

[43] D. Gidaspow, R. Bezburuah, and J. Ding, *Hydrodynamics of Circulating Fluidized Beds: Kinetic Theory Approach (No. CONF-920502-1)*, Chicago, IL (United States), Illinois Inst. of Tech., Dept. of Chemical Engineering, 1991.

[44] C. E. Brennen, *Fundamentals of Multiphase Flow*, Cambridge University Press, 2005.

[45] P. C. Johnson and R. Jackson, “Frictional–collisional constitutive relations for granular materials, with application to plane shearing,” *J. Fluid Mech.*, vol. 176, pp. 67–93, 1987. https://doi.org/10.1017/s0022112087000570.

[46] T. Jin, Y. J. Li, Z. B. Liang, Y. Q. Lan, G. Lei, and X. Gao, “Numerical prediction of flow characteristics of slush hydrogen in a horizontal pipe,” *Int. J. Hydrogen Energy*, vol. 42, no. 6, pp. 3778–3789, 2017. https://doi.org/10.1016/j.ijhydene.2016.09.054.

[47] D. Vuarnoz, O. Sari, P. W. Egolf, and H. Liardon, “Ultrasonic velocity profiler UVP-XW for ice-slurry flow characterisation,” in *Proceedings of the Third International Symposium on Ultrasonic Doppler Method for Fluid Mechanics and Fluid Engineering*, Lausanne, Switzerland, 2002.

Q1 [48] R. G. Gillies, C. A. Shook, and J. Xu, “Modelling heterogeneous slurry flows at high velocities,” *Can. J. Chem. Eng.*, vol. 82, no. 5, pp. 1060–1065, 2004. https://doi.org/10.1002/cjce.5450820523.

Footnotes

Text Footnotes

Research ethics: Not Applicable.

Author contributions: ~~Conceptualization, KSR, PB, VSB, NB, LR, SS; formal analysis, KSR, PB, VSB, NB, LR, SS; investigation, KSR, PB, VSB, NB, LR, SS; writing~~ Conceptualization, KSR, PB, VSB, NB, LR; formal analysis, KSR, PB, VSB, NB, LR, SS; investigation, KSR, PB, VSB, NB, LR; writing ~~– original draft preparation, KSR, PB, VSB, NB, LR, SS; writing~~ original draft preparation, KSR, PB, VSB, NB, LR; writing ~~– review and editing, KA, DNT, VNR, EESM; project~~

~~administration, KA, DNT, VNR, EESM; funding acquisition, KA, DNT, VNR, EESM. All authors have read and agreed to the published version of the manuscript. All authors have read and agreed to the published version of the manuscript.~~review and editing, SS, KA, DNT, VNR, EESM; project administration, KA, DNT, VNR, EESM; funding acquisition, KA, DNT, VNR, EESM. All authors have read and agreed to the published version of the manuscript. All authors have read and agreed to the published version of the manuscript.

Conflict of interest: The authors declare no competing interests.

Research funding: The authors extend their appreciation to the Deanship of Scientific Research at King Khalid University for funding this work through large group Research Project under grant number RGP2/28/44.

Q8

Data availabilQ9**:** ~~My manuscript has no associated data.~~ All the characterizations, analysis, testing's related works, and testing's have been provided by Prabhakar Bhandari and Lalit Ranakoti. Additionally, the raw data can be obtained on request from the corresponding authors, Prabhakar Bhandari and Lalit Ranakoti.

Queries and Answers

Q1

Query: Please note that the short title will be used as running head on top of the pages. Please check the retained short title or kindly provide the short title fewer than 75 characters including space.

Answer: I confirm the same.

Q2

Query: Please confirm that the forename(s) and surname(s) have been identified correctly and please carefully verify the spelling of all authors' names.

Answer: I confirm the same.

Q3

Query: As per De Gruyter policy, no author list changes are permitted after acceptance of an article. The De Gruyter production team is instructed to enforce this policy during the production/proofing process.

Answer: I confirm the same as the authors have not made any sort of changes in the authors, authorship order, or removing/adding any authors from the accepted version of the manuscript.

Q4

Query: As per journal style, author names in the author group must have forename and last name in full with middle name as initials if given. First initials are not permitted, unless author provides full middle name as name of use. Kindly check and provide the full first name and last name for the authors "N. Beemkumar and Karthikeyan A."

Answer: I confirm the same as I have added the full names.

Q5

Query: Please note that as per the journal style, only one email address should be included for the corresponding author "Shubham Sharma". Kindly check and advise on the one to be retained.

Answer: Kindly consider only one mail as mentioned below,

shubham543sharma@gmail.com

Q6

Query: We expect a figure caption with a main title followed by the description of the part labels. Hence, could you please provide main captions for the figure 3 in this format to proceed.

Answer: Modified

Q7

Query: Figure 12 was not cited in the text. Please check that the citations suggested are in the appropriate place, and correct if necessary.

Answer: Modified

Q8

Query: Please note that the funding information in the □Acknowledgements□ section has been moved to □Research funding□, kindly check and amend if necessary.

Answer: Acknowledgment: The authors extend their appreciation to the Deanship of Scientific Research at King Khalid University for funding this work through large group Research Project under grant number RGP2/28/44.

Q9

Query: Please note that we have received the Template for Ethical and Legal Declarations for author statements for this item without the headings "Informed consent, Use of Large Language Models, AI and Machine Learning Tools" Please check and provide the missing headings following style. You can download the template here: https://degruyter.knack.com/joda-20#template-for-ethical-and-legal-declarations/.

Answer:

Informed consent: Not applicable.

Use of Large Language Models, AI and Machine Learning Tools: None declared.

Q10

Query: Please supply the issue number for the references "4, 7-9, 13, 14, 20-22, 24, 26-29, 31, 35-39, 42, 45".

Answer:

Q11

Query: References [21] and [40] were identical, hence the latter has been removed from the reference list and subsequent references have been renumbered both in the list and in the citations. Please check and amend, if required.

Answer:

Q12

Query: Please supply the name of the city for the references “40, 44”.

Answer: